Available online at www.sciencedirect.com
SCIENCE DIRECT®
Journal of Organometallic Chemistry 683 (2003) 388–397
Journal of Organometallic Chemistry
www.elsevier.com/locate/jorganchem

Further studies of tetrakis(*N*,*N*′-dialkylbenzamidinato)diruthenium(III) chloro and alkynyl compounds: molecular engineering of metallayne monomers

Guo-Lin Xu, Conrad G. Jablonski, Tong Ren *

Department of Chemistry, University of Miami, Coral Gables, FL 33124, USA

Received 29 April 2003

Abstract

Three diruthenium(III) compounds $Ru_2(\mathbf{L})_4Cl_2$, where **L** is *m*MeODMBA (*N*,*N*′-dimethyl-3-methoxybenzamidinate, **1a**), DiMeODMBA (*N*,*N*′-dimethyl-3,5-dimethoxy benzamidinate, **1b**), or DEBA (*N*,*N*′-diethylbenzamidinate, **1c**), were prepared from the reactions between $Ru_2(OAc)_4Cl$ and respective H**L** under reflux conditions. Metathesis reactions between **1** and LiC_2Y resulted in bis-alkynyl derivatives $Ru_2(\mathbf{L})_4(C_2Y)_2$ [Y = Ph (**2**), $SiMe_3$ (**3**), Si^iPr_3 (**4**) and C_2SiMe_3 (**5**)]. The parent compounds **1** are paramagnetic ($S = 1$), while bis-alkynyl derivatives **2**–**5** are diamagnetic and display well-solved ^{1}H- and ^{13}C-NMR spectra. Molecular structures of compounds **1b**, **1c**, **2c**, **3c** and **4b** were established through single crystal X-ray diffraction studies, which revealed Ru–Ru bond lengths of ca. 2.32 Å for parent compounds **1** and 2.45 Å for bis-alkynyl derivatives. Cyclic voltammograms of all compounds feature three one-electron couples: an oxidation and two reductions, while the reversibility of observed couples depends on the nature of axial ligands.

Keywords: Diruthenium; Metallayne; Alkynylation; *N*,*N*′-Dialkylbenzamidinate

1. Introduction

There is a continued interest in our laboratory to construct *molecular electronic wires* based on diruthenium paddlewheel species bearing axial alkynyl ligands [1]. These diruthenium species are attractive because of their rich redox activities, high degree of electron mobility along Ru_2–$(CC)_m$– backbone, and amenability to divergent/convergent synthesis [2–12]. In addition, these compounds may be useful for applications such as molecular luminescent materials [13], nonlinear optical materials [14], and building blocks for supramolecular assemblies [15–18].

For applications in electronic and opto-electronic materials, it is critical to maintain a long-range electronic coupling (or conjugation) along the backbone of molecules. It has been established that extensive electronic couplings between [M] termini exist in the type **I** dimer with M as $Ru_2(ap)_4$ (Scheme 1, *ap* = 2-anilinopyridinate), but the coupling strength decreases exponentially as the distance between two [M] increases [2,3]. A possible strategy to maintain coupling strength over a long distance is to use oligomeric metallaynes (**II** in Scheme 1) of a minimal number of acetylenic units (*m*) between adjacent [M] units. In the case of diruthenium metallaynes based on either *ap* or *D*Ar*F* (diarylformamdinate) supporting ligand [1], the minimal *m* appears to be 4 due to the presence of aryls flanking one or both axial positions of the Ru_2 core.

To address the issue of steric crowding around axial positions, we introduced a new family of diruthenium(III) compounds based on *N*,*N*′-dimethylbenzamidinate (DMBA) recently [12], where the first bis-trimethylsilylacetylide compound on a Ru_2 core was realized. Although $Ru_2(DMBA)_4(C_{2k}H)_2$ ($k = 1$, 2) compounds are soluble in common organic solvents, oligomers/polymers obtained from oxidative coupling of these compounds are much less soluble, making chro-

* Corresponding author. Tel.: +1-305-2846617; fax: +1-305-2841880.
E-mail address: tren@miami.edu (T. Ren).

0022-328X/03/$ - see front matter © 2003 Elsevier B.V. All rights reserved.
doi:10.1016/j.jorganchem.2003.08.005

Scheme 1. Conjugated metallayne dimer **I** and oligomer **II**.

matographic separation nearly impossible [19]. In addition, it was noted that $Ru_2(DMBA)_4(C_{2k}R)_2$ (R as H or silyl) compounds display poor stability towards reduction that is attributed to the Ru–C bond cleavage [12]. To improve both the solubility of Ru_2–metallaynes and redox stability of the Ru–C bonds, diruthenium(III) compounds based on derivatized DMBA ligands are being explored. Reported herein are the synthesis and characterization of diruthenium(III) compounds $Ru_2(\mathbf{L})_4Cl_2$, and their bis(ethynyl) and bis(butadiynyl) derivatives based on three modified DMBA ligands: *m*MeODMBA (*N*,*N*′-dimethyl-3-methoxybenzamidinate), DiMeODMBA (*N*,*N*′-dimethyl-3,5-dimethoxybenzamidinate), DEBA (*N*,*N*′-diethylbenzamidinate), (Scheme 2 and Table 1).

2. Results and discussion

2.1. Synthesis

Similar to the previously reported synthesis of $Ru_2(DMBA)_4Cl_2$ [12], refluxing $Ru_2(OAc)_4Cl$ with five equivalents of ligands, Et_3N and LiCl in THF for 2 h (overnight in the case of DEBA) resulted in compounds $Ru_2(\mathbf{L})_4Cl_2$ (**L**: *m*MeODMBA, **1a**; DiMeODMBA, **1b**; DEBA, **1c**) in nearly quantitative yields. Although the presence of *N*-ethyl groups in DEBA slows down the substitution reaction, it does not affect the yield of **1c**. While these compounds cannot be characterized using NMR spectra because of their paramagnetisms, their compositions were ascertained through both FABMS and combustion analysis. Further confirmations were achieved with single-crystal X-ray diffraction study of compounds **1b** and **1c**.

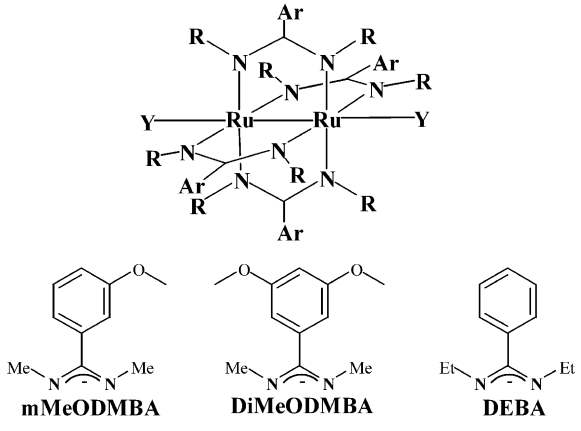

Scheme 2. Derivatized DMBA ligands and their Ru_2 compounds.

Table 1
Designation of compounds **1**–**5**

Y	Cl	C_2Ph	C_2SiMe_3	$C_2Si^iPr_3$	C_4SiMe_3
*m*MeODMBA	**1a**		**3a**	**4a**	**5a**
DiMeODMBA	**1b**	**2b**	**3b**	**4b**	**5b**
DEBA	**1c**	**2c**	**3c**	**4c**	**5c**

Compounds **1** readily reacted with lithiated acetylenes (LiC_2Y) to afford corresponding bis-acetylide derivatives in nearly quantitative yields. On the other hand, reactions between **1** and lithiated butadiynyl (LiC_4SiMe_3) produced both $Ru_2(\mathbf{L})_4(C_4SiMe_3)_2$ (**5**) and trace amounts of corresponding mono- and di-desilylated compounds. Consequently, compounds **5** were isolated in reduced yields after column chromatographic purifications. The ease of desilylation of **5** is attributed to a much enhanced electron deficiency of butadiynyl ligand in comparison with ethynyl ligand [12]. Compared with the previously reported DMBA-based compounds [12], the solubility of bis-alkynyl derivatives **2**–**5** has been markedly improved by the modification of either the phenyl ring or *N*-alkyl. Bis-alkynyl adducts of the $Ru_2(m\text{MeODMBA})_4$ core are even soluble in hexanes. Interestingly, introduction of the second *m*-OMe phenyl substituent does not provide additional solubility enhancement.

Compounds **1a**–**c** are paramagnetic with room temperature magnetic moments of 2.89, 3.09, 2.63 μ_B, respectively, which are indicative of an $S = 1$ ground state as in the cases of $Ru_2(DMBA)_4Cl_2$ [12] and $Ru_2(hpp)_4Cl_2$ [20]. Bis-alkynyl derivatives **2**–**5** are all diamagnetic, and well-resolved ^{1}H- and ^{13}C-NMR spectra were obtained. Compounds **1** exhibit two intense bands in visible–near-infrared (Vis–NIR) spectra centered at ca. 430 and 760 nm, which account for the deep brown color of these compounds. Upon the formation of bis-alkynyl both bands were red-shifted to ca. 490 and 860 nm, which resulted in a deep red color for compounds **2**–**5**. Although the exact natures of these excitations remain unclear, they probably contain a charge-transfer component judging from the intensities. Vis–NIR spectra for compounds **1**–**5** are provided in supporting information.

2.2. Molecular structures

Among 14 compounds reported herein, single crystal X-ray diffraction studies were performed for chloro-complexes **1b** and **1c**, and acetylide complexes **2c**, **3c**, and **4b**, and structural plots are shown in Figs. 1–6, respectively. Clearly, all the compounds adopt the paddlewheel motif with four *N*,*N*′-bidentate bridging ligands occupying the equatorial positions and two chloro/alkynyl ligands occupying the axial positions.

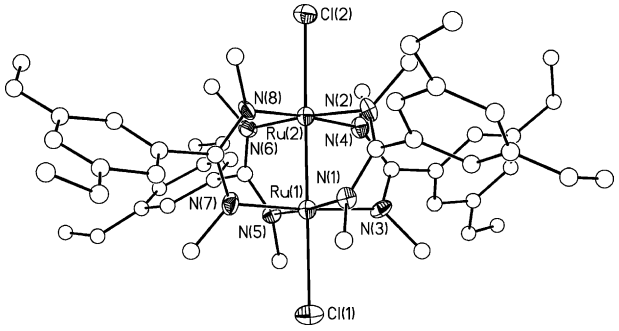

Fig. 1. ORTEP plot of molecule **1b** at 30% probability level.

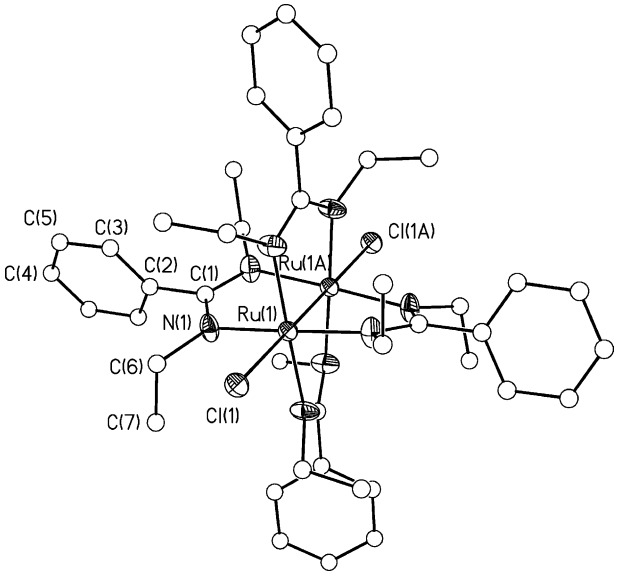

Fig. 2. ORTEP plot of molecule **1c** at 30% probability level.

Compound **1b** crystallizes in a monoclinic space group, and the asymmetric unit consists of one independent molecule. Compound **1c** crystallizes in a body-centered tetragonal space group, and the asymmetric unit only contains one-eighth of **1c**. The Ru–Ru bond length in compound **1b** (2.316(1) Å) is similar to those found for $Ru_2(DMBA)_4Cl_2$ (2.322(1) Å) [12] and $Ru_2(hpp)_4Cl_2$ (2.321 Å) [20], while the Ru–Ru bond in compound **1c** (2.340(1) Å) is slightly longer. The Ru–Cl bond lengths in both **1b** (2.568[3] Å) and **1c** (2.597(2) Å) are comparable to that in $Ru_2(DMBA)_4Cl_2$ (2.557(1) Å), but are shorter than that in $Ru_2(hpp)_4Cl_2$ (2.705 Å). Since Ru–Cl bond lengths in compounds **1** are about the same as the sum of ionic radii of Ru^{3+} and Cl^- (2.58 Å) but much larger than the sum of covalent radii of Ru and Cl (2.23 Å) [21], the Ru–Cl bond in these compounds is best described as ionic. Lack of covalent bonding between Ru and Cl centers implies that the σ(Ru–Ru) bond is retained. Clearly, the ground state configuration of $Ru_2(\mathbf{L})_4Cl_2$ is best described as $\sigma^2\pi^4\delta^2\pi^{*2}$, and the diruthenium core is triply bonded

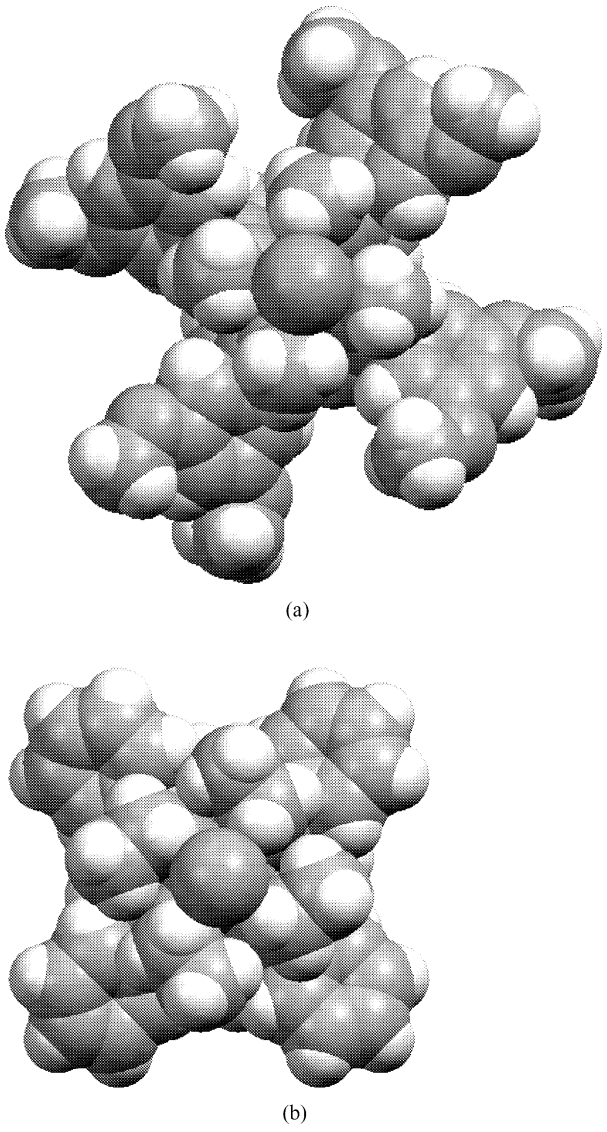

(a)

(b)

Fig. 3. Space-filling plots of **1b** (a) and **1c**, viewed along Ru–Ru vectors.

Table 2
Selected bond lengths (Å) and angles (°) for molecules **1b** and **1c**

1b		**1c**	
Bond lengths			
Ru(2)–Ru(1)	2.316(1)	Ru(1)–Ru(1)′	2.340(1)
Ru(1)–Cl(1)	2.571(3)	Ru(1)–Cl(1)	2.597(2)
Ru(2)–Cl(2)	2.564(3)	Ru(1)–N(1)	2.054(4)
Ru(1)–N(1)	2.038(8)		
Ru(1)–N(3)	2.063(8)		
Ru(1)–N(5)	2.049(9)		
Ru(1)–N(7)	2.047(8)		
Ru(2)–N(2)	2.046(8)		
Ru(2)–N(4)	2.042(8)		
Ru(2)–N(6)	2.035(8)		
Ru(2)–N(8)	2.021(8)		
Bond angles			
Ru(2)–Ru(1)–Cl(1)	179.8(1)	Ru(1)′–Ru(1)–Cl(1)	180.000(1)
Ru(1)–Ru(2)–Cl(2)	178.8(1)		

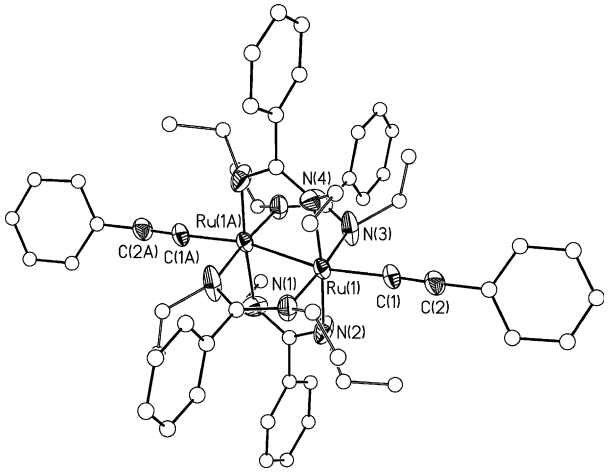

Fig. 4. ORTEP plot of molecule **2c** at 30% probability level.

[22]. Selected bond lengths and angles for molecules **1b** and **1c** are listed in Table 2.

It was hoped that the introduction of *N*-ethyl group in DEBA would lead to a better hydrophobic pocket around the axial positions of Ru_2 core than that of *N*-methyl analog, and consequently form a steric protection of the Ru–C bond. To verify this hypothesis, space-filling plots of both compounds **1b** and **1c** viewed along Ru–Ru vectors were generated and shown in Fig. 3. It is clear that the *N*-ethyl groups in **1c** indeed form dense coverage around the Ru–Cl bond in comparison with **1b**.

Ru–Ru bond lengths in bis-acetylide derivatives **2c** (2.458(1) Å), **3c** (2.461(1) Å), and **4b** (2.476(1) Å) are about the same as those reported for bis-alkynyl compounds of $Ru_2(DMBA)_4$ core (ca. 2.45 Å) [12], but much longer than that found for respective parent molecules (2.31–2.34 Å). The Ru–C distances range between 1.965 and 1.993 Å, indicating the formation of a strong σ(Ru–C) bond at the expense of σ(Ru–Ru) bond. Hence, the ground state configuration for bis-alkynyl compounds should be $\pi^4\delta^2\pi^{*4}$ instead of the $\sigma^2\pi^4\delta^2\pi^{*2}$ assigned to the parent molecules [23]. Selected bond lengths and angles for compounds **2c**, **3c** and **4b** are listed in Table 3.

Table 3 reveals a significant variation among Ru–N bond lengths in each of bis-acetylide compounds. The variation, however, is not random: there is always a pair of shortened Ru–N bonds on each Ru center, which are trans to a pair of elongated Ru–N bonds on the same Ru. Concurrently, the Ru–Ru–C angles are also significantly deviated from 180°. Such structural distortion around the first coordination sphere of Ru_2 core has been prevalent in bis-alkynyl compounds of a diruthenium(III) core [4,6,9,10,12,20], and is attributed to a second order Jahn-Teller effect [10]. It is also clear from Table 3 that structural distortions in both **2c** and **4b** are far more drastic than that in **3c**, indicating that the *N*-ethyl groups in **3c** have played a role in suppressing the second order Jahn-Teller effect.

2.3. Electrochemistry

Similar to diruthenium species supported by *D*Ar*F* and *ap* ligands [1], compounds **1**–**5** are highly redox active, as evident from the cyclic voltammograms (CV) of compounds **na** (**n** = **1**, **3**–**5**) in Fig. 7. Other compounds reported herein (**nb** and **nc**) exhibit similar CVs, which are included in Section 5. CVs in Fig. 7 generally feature three one electron waves: a quasi-reversible oxidation (**A**), a quasi-reversible reduction (**B**), and an irreversible reduction (**C**). All the couples are Ru_2-based and assignments are outlined in Scheme 3 below. It is

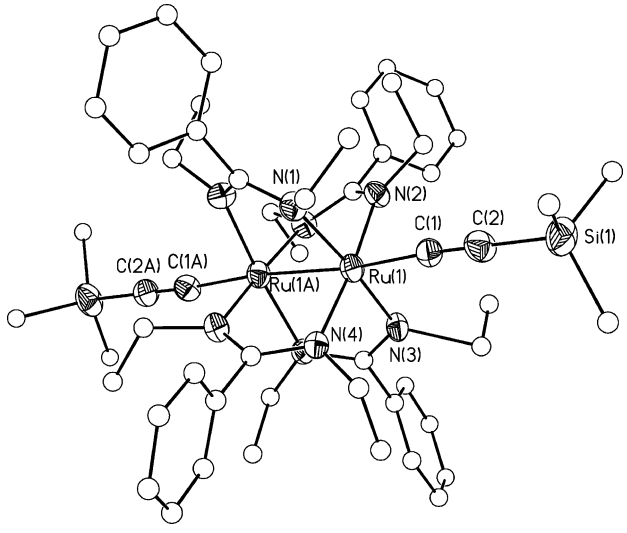

Fig. 5. ORTEP plot of molecule **3c** at 30% probability level.

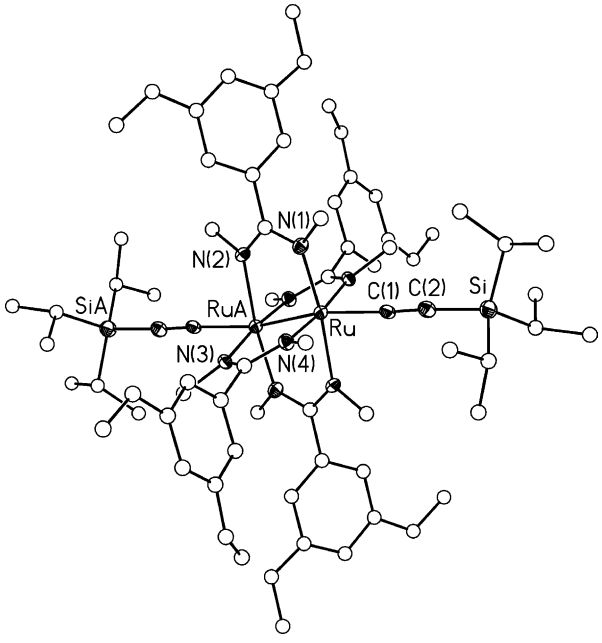

Fig. 6. ORTEP plot of molecule **4b** at 30% probability level.

Table 3
Selected bond lengths (Å) and angles (°) for molecules **2c**, **3c** and **4b**

2c		**3c**		**4b**	
Bond lengths					
Ru(1)–Ru(1′)	2.4588(9)	Ru(1)–Ru(1′)	2.4612(5)	Ru–Ru′	2.4760(7)
Ru(1)–N(1)	1.982(5)	Ru(1)–N(1)	2.074(4)	Ru–N(1)	1.993(3)
Ru(1)–N(2)	2.007(5)	Ru(1)–N(2)	2.088(4)	Ru–N(2)	2.137(3)
Ru(1)–N(3)	2.108(5)	Ru(1)–N(3)	2.023(4)	Ru–N(3)	2.116(3)
Ru(1)–N(4)	2.103(5)	Ru(1)–N(4)	2.034(4)	Ru–N(4)	1.994(3)
Ru(1)–C(1)	1.984(6)	Ru(1)–C(1)	1.965(3)	Ru–C(1)	1.991(4)
C(1)–C(2)	1.192(8)			C(1)–C(2)	1.205(6)
Bond angles					
C(1)–Ru(1)–Ru(1)′	168.3(2)	C(1)–Ru(1)–Ru(1)	173.8(1)	C(1)–Ru–Ru′	161.0(1)

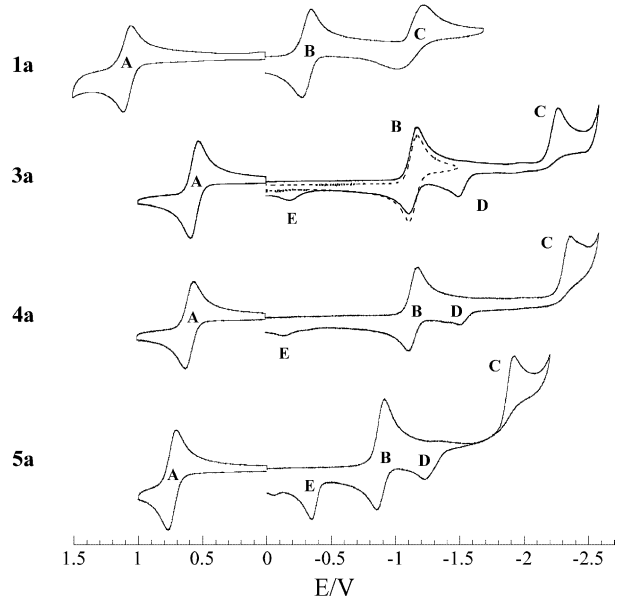

Fig. 7. CVs of compounds **1a**, **3a**, **4a** and **5a** recorded in 0.20 M THF solution of Bu_4NPF_6 at a scan rate of 0.10 V s^{-1}.

clear from Fig. 7 that the integrity of bis-alkynyl compounds is affected by electrochemical reductions. As shown for **3a**, the first reduction was reversible when the potential sweep window was limited to −1.5 V. Upon the inclusion of the second reduction, new waves **D** and **E** appeared on the returning sweep, which are attributed to the degradation products of the reduced metallayne, as outlined in Scheme 3. Other bis-alkynyl compounds behave similarly. Notably, those based on DEBA (**2c**–**5c**) do not show marked enhancement of redox stability in comparison with compounds **2a/b**–**5a/b**. Clearly, the origin of Ru–C bond cleavage is electronic, not steric, in nature.

Several trends are clear based on the comparison of CVs in Fig. 7 and data in Table 4. The redox couples of bis-alkynyl compounds are cathodically shifted relative to their parental chloro compounds **1**, and the potential shift is attributed to the strong donor nature of alkynyl ligands. Electrode potentials of ethynyl compounds **2**–**4** fall within a very narrow range with those based on DEBA ligands being most positive. Couples of bis-butadiynyl compounds are ca. 200 mV more positive than the corresponding couples of bis-ethynyl compounds, consistent with the fact that butadiynyl is more electron-deficient than ethynyl. Availability of electrode potentials for both the one electron oxidation and reduction enables the estimation of *electrochemical* HOMO–LUMO gap (E_g) according to equation $E_g = E(+1/0) - E(0/-1)$ [24], and the calculated values are also listed in Table 4. The E_g values for chloro-, ethynyl and butadiynyl compounds are narrowly centered at 1.40, 1.71 and 1.63 V, respectively, while the corresponding optical gaps (E_{op}) are ca. 1.65, 1.45, and 1.42 eV, respectively. These gaps, although larger than those reported for both the *ap* and *D*Ar*F* based compounds [1], are still fairly small in comparison with those found for the monomers of well-known conjugated organic oligomers, such as oligo(phenylene-ethynylene) and oligo(phenylene-vinylene) [25,26].

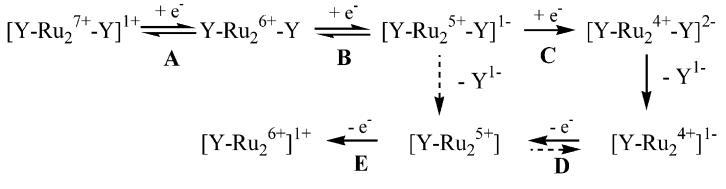

Scheme 3. Electrochemical and chemical steps in $Ru_2(\mathbf{L})Y_2$; Y = Cl and alkynyl.

Table 4
Comparison of electrode potentials and optical energy gaps among $Ru_2(\mathbf{L})_4\mathbf{Y}_2$

L	Y	$E(+1/0)$ (V)	$E(0/-1)$ (V)	E_g (V)	E_{op} (eV)
hpp [20][a]	Cl	0.55	−0.60	1.15	1.61
DMBA [12]	Cl	1.058	−0.326	1.38	1.68
*m*MeODMBA	Cl	1.078	−0.323	1.40	1.59
DiMeODMBA	Cl	1.108	−0.322	1.43	1.60
DEBA	Cl	1.205	−0.163	1.37	1.67
DMBA [12]	C_2TMS	0.553	−1.146	1.70	1.42
*m*MeODMBA	C_2TMS	0.560	−1.150	1.71	1.45
DiMeODMBA	C_2TMS	0.559	−1.150	1.71	1.45
DEBA	C_2TMS	0.625	−1.085	1.71	1.50
DMBA [12]	C_4TMS	0.730	−0.897	1.63	1.40
*m*MeODMBA	C_4TMS	0.737	−0.880	1.62	1.41
DiMeODMBA	C_4TMS	0.725	−0.900	1.62	1.41
DEBA	C_4TMS	0.777	−0.860	1.64	1.46

[a] The potential reported in that work was measured in CH_2Cl_2 containing 0.1 M TMAP.

3. Conclusions

Modification of the DMBA ligand through the introduction of either one or two *m*-MeO phenyl substituents drastically improved the solubility of $Ru_2(\mathbf{L})_4Y_2$ compounds, while electrochemical and optical properties of resultant compounds were not altered. Replacing *N*-methyl with *N*-ethyl, however, did not result in an enhancement of the stability of Ru–C bond. To achieve the latter objective, a significant reduction in the electron-richness of the Ru_2-core appears necessary.

4. Experimental

Phenylacetylene, 1,4-bistrimethylsilyl-1,3-butadiyne, trimethylsilylacetylene, triisopropylsilylacetylene and ^{n}BuLi were purchased from Aldrich, and silica gel from Merck. *N*,*N*′-dimethyl-3-methoxybenzamidine, *N*,*N*′-dimethyl-3,5-dimethoxybenzamidine, *N*,*N*′-diethylbenzamidine were prepared according to a modified literature procedure [27], which will be reported separately [28]. THF was distilled over Na–benzophenone under an N_2 atmosphere prior to use. ^{1}H- and ^{13}C-NMR spectra were recorded on a Bruker AVANCE300 NMR spectrometer, with chemical shifts (δ) referenced to the residual $CHCl_3$ and the solvent $CDCl_3$, respectively. Infrared spectra were recorded on a Perkin–Elmer 2000 FT-IR spectrometer using KBr disks. Vis–NIR spectra in THF were obtained with a Perkin–Elmer Lambda-900 UV–vis–NIR spectrophotometer. CVs were recorded in 0.2 M (^{n}Bu)$_4$NPF$_6$ solution (THF, N_2-degassed) on a CHI620A voltammetric analyzer with a glassy carbon working electrode (diameter = 2 mm), a Pt-wire auxiliary electrode and a Ag | AgCl reference electrode. The concentration of diruthenium species is always 1.0 mM. The ferrocenium–ferrocene couple was observed at 0.568 V (vs. Ag | AgCl) under experimental conditions.

4.1. Synthesis of $Ru_2(L)_4Cl_2$

Preparation of Ru_2(*m*MeODMBA)$_4Cl_2$ (**1a**). A 200 ml flask was charged with $Ru_2(OAc)_4Cl$ (0.950 g, 2.0 mmol), H*m*MeODMBA (1.78 g, 10 mmol), LiCl (excess), Et_3N (1 ml) and THF (100 ml). The mixture was refluxed for 2 h to yield a dark brown solution. After solvent removal, the residue was dissolved in CH_2Cl_2 and filtered through a 2-cm sil-gel pad (deactivated with Et_3N). Recrystallization from THF–hexanes yielded **1a** as a dark brown solid (1.85 g, 94% based on Ru). Data for **1a**: Anal. for $C_{40}H_{52}Cl_2N_8O_4Ru_2\cdot 0.5$THF Found (Calc.): C, 49.26 (49.56); H, 5.56 (5.51); N, 10.65 (11.01)%; FABMS (*m*/*e*, based on ^{101}Ru): 982 [M$^+$H]; Vis–NIR, λ_{max} (nm, ε (M^{-1} cm^{-1})): 781 (7,260), 510(sh), 428 (6,510); IR, ν (cm^{-1}): 2918, 2836, 1578, 1466, 1429, 1286, 1247, 1035, 880, 865, 796, 498; Electrochemistry, $E_{1/2}$ (V), ΔE_p (V), $i_{backward}/i_{forward}$: **A**, 1.078, 0.059, 0.829; **B**, −0.323, 0.067, 0.934; **C**, −1.237, N/A, N/A.

Ru_2(DiMeODMBA)$_4Cl_2$ (**1b**) was prepared using the same procedure as that for **1a** and replacing H*m*MeODMBA with HDiMeODMBA in 95% yield based on Ru. Data for **1b**: Anal. for $C_{44}H_{60}Cl_2N_8O_8Ru_2$ Found (Calc.): C, 47.39 (47.96); H, 5.42 (5.45); N, 9.61 (10.17)%; FABMS (*m*/*e*, based on ^{101}Ru): 1102 [M$^+$H]; Vis–NIR, λ_{max} (nm, ε(M^{-1} cm^{-1})): 774 (6,240), 506(sh), 427 (5,500); IR, ν (cm^{-1}): 2938, 2838, 1592, 1465, 1425, 1400, 1205, 1157, 1033, 877, 498; Electrochemistry, $E_{1/2}$ (V), ΔE_p (V), $i_{backward}/i_{forward}$: **A**, 1.108, 0.108, 0.593; **B**, −0.322, 0.065, 0.991; **C**, −1.242, N/A, N/A.

Ru_2(DEBA)$_4Cl_2$ (**1c**) was prepared using the same procedure as that for **1a** and replacing H*m*MeODMBA with HDEBA and a longer refluxing time (ca. 10 h) in

96% yield based on Ru. Data for **1c**: Anal. for $C_{44}H_{60}Cl_2N_8Ru_2$ Found (Calc.): C, 53.51 (54.27); H, 6.15 (6.17); N, 11.32 (11.51)%; FABMS (*m*/*e*, based on ^{101}Ru): 939 [$M^+ - Cl$]; Vis–NIR, λ_{max} (nm, ε (M^{-1} cm^{-1})): 742 (5,570), 498 (2,750), 429 (3,640); IR, *v* (cm^{-1}): 2987, 2957, 2954, 2864, 1640, 1474, 1420, 1350, 1291, 1261, 1140, 1073, 1054, 1023, 816, 802, 770, 730, 706, 527, 467; Electrochemistry, $E_{1/2}$ (V), ΔE_p (V), $i_{backward}/i_{forward}$: **A**, 1.205, 0.059, 0.647; **B**, −0.163, 0.121, 0.955; **C**, −1.198, N/A, N/A.

4.2. Reactions between $Ru_2(L)_4Cl_2$ and $LiC_{2n}Y$

Preparation of Ru_2(*m*MeODMBA)$_4$(C_2TMS)$_2$ (**3a**). To a 40 ml THF solution of Ru_2(*m*MeODMBA)$_4Cl_2$ (0.196 g, 0.20 mmol) was added 5 equiv. of LiC_2TMS (prepared from treating 1 mmol TMSCCH with 0.63 ml 1.6 M ^{n}BuLi) at room temperature (r.t.). The reaction mixture was stirred under argon for 1 h, followed by filtration through a 2 cm silica pad to yield a dark red solution. After solvent removal, the residue was washed with copious amount of methanol and dried under vacuum overnight to yield 0.190 g red powder (**3a**, 86% based on Ru). Data for **3a**: Anal. for $C_{50}H_{70}N_8O_4Si_2Ru_2\cdot$THF, Found (Calc.): C, 55.69 (55.10); H, 6.33 (6.63); N, 9.20 (9.52)%. ^{1}H-NMR: 7.34 (*t*, 4H, aromatic), 6.89 (*q*, 4H, aromatic), 6.56–6.48 (*m*, 8H, aromatic), 3.80 (*s*, 12H, CH_3O–), 3.23 (*s*, 24H, CH_3N–), 0.02 (s, 18H, (CH_3)$_3$Si–); ^{13}C-NMR (C≡C): 135.2, 99.4; FABMS (*m*/*e*, based on ^{101}Ru): 1107 [M^+H]; Vis–NIR, λ_{max} (nm, ε (M^{-1} cm^{-1})): 857 (2,610), 491 (15,490); IR, *v*(C≡C) (cm^{-1}): 2000(s); Electrochemistry, $E_{1/2}$ (V), ΔE_p (V), $i_{backward}/i_{forward}$: **A**, 0.560, 0.067, 0.981; **B**, −1.150, 0.067, 0.558; **C**, −2.279, N/A, N/A; **D**, −1.497, N/A, N/A.

Preparation of Ru_2(*m*MeODMBA)$_4$(C_2Tips)$_2$ (**4a**) was undertaken using the same procedure as that for **3a** and replacing LiC_2TMS with LiC_2Tips in 76% yield. Data for **4a**: Anal. for $C_{62}H_{94}N_8O_4Si_2Ru_2\cdot 2CH_2Cl_2\cdot H_2O$, Found (Calc.): C, 52.41 (52.60); H, 6.95 (6.85); N, 7.08 (7.66)%. ^{1}H-NMR: 7.34 (*t*, 4H, aromatic), 6.90 (*m*, 4H, aromatic), 6.57–6.47 (*m*, 8H, aromatic), 3.78 (*s*, 12H, CH_3O–), 3.27 (*s*, 24H, CH_3N–), 1.07–0.85 (m, 42H, (C_3H_7)$_3$Si–); ^{13}C-NMR (C≡C): 125.9, 71.0; FABMS (*m*/*e*, based on ^{101}Ru): 1274 [M^+H]; Vis–NIR, λ_{max} (nm, ε (M^{-1} cm^{-1})): 855 (1,800), 490 (11,470); IR, *v*(C≡C) (cm^{-1}): 2001(s); Electrochemistry, $E_{1/2}$ (V), ΔE_p (V), $i_{backward}/i_{forward}$: **A**, 0.587, 0.067, 0.967; **B**, −1.157, 0.079, 0.642; **C**, −2.379, N/A, N/A; **D**, −1.512, N/A, N/A.

Preparation of Ru_2(*m*MeODMBA)$_4$(C_4TMS)$_2$ (**5a**) was undertaken using the same procedure as that for **3a** and replacing LiC_2TMS with LiC_4TMS. Silica column chromatography was used to separate **5a** (68%) from trace amounts of *trans*-(TMSC_4)Ru_2(*m*-MeODMBA)$_4$(C_4H) and Ru_2(*m*MeODMBA)$_4$(C_4H)$_2$. Data for **5a**: Anal. for $C_{54}H_{70}N_8O_4Ru_2Si_2\cdot 2C_6H_{14}$ Found (Calc.): C, 60.60 (59.82); H, 7.18 (7.40); N, 7.81 (8.45). ^{1}H-NMR: 7.32 (*t*, 4H, aromatic), 6.95 (*s*, 2H, aromatic), 6.92–6.88 (*q*, 4H, aromatic), 6.50 (*d*, 3H, aromatic), 6.44 (*s*, 3H, aromatic), 3.77 (*d*, 12H, CH_3O–), 3.19 (*s*, 24H, CH_3N–), 0.09 (s, 18H, –Si(CH_3)$_3$); ^{13}C-NMR (C≡C): 128.7, 108.7, 90.1, 75.9; FABMS (*m*/*e*, based on ^{101}Ru): 1154 [M^+]; Vis–NIR, λ_{max} (nm, ε (M^{-1} cm^{-1})): 880 (1,360), 513 (7,290); IR, *v*(C≡C) (cm^{-1}): 2160(*m*), 2106(*s*); Electrochemistry, $E_{1/2}$ (V), ΔE_p (V), $i_{backward}/i_{forward}$: **A**, 0.737, 0.072, 0.909; **B**, −0.880, 0.062, 0.644; **C**, −1.922, N/A, N/A; **D**, −1.227, N/A, N/A.

Preparation of Ru_2(DiMeODMBA)$_4$(C_2Ph)$_2$ (**2b**). To a 40 ml THF suspension of Ru_2(DiMeODMBA)$_4Cl_2$ (0.220 g, 0.2 mmol) was added 5 equiv. of LiCCPh (prepared from 1.0 mmol of PhCCH and 0.63 ml 1.6 M ^{n}BuLi) at r.t. The reaction mixture was stirred under argon for 2 h, followed by filtration through a 2 cm silica pad to yield a dark red solution. After solvent removal, the residue was washed with copious amount of methanol and hexanes and dried under vacuum overnight to yield **2b** as red microcrystalline solid (0.217 g, 96%). Data for **2b**: Anal. for $C_{60}H_{70}N_8O_8Ru_2\cdot C_6H_{14}$ Found (Calc.): C, 60.36 (60.09); H, 6.18 (6.37); N, 7.85 (8.49)%. ^{1}H-NMR: 7.17–7.09 (*m*, 8H, aromatic), 6.89 (*t*, 2H, aromatic), 6.45 (*t*, 4H, aromatic), 6.10 (*d*, 8H, aromatic), 3.76 (*s*, 24H, CH_3O–), 3.29 (*s*, 24H, CH_3N–); ^{13}C-NMR (C≡C): 128.2, 67.4; FABMS (*m*/*e*, based on ^{101}Ru): 1234 [M^+H]; Vis–NIR, λ_{max} (nm, ε (M^{-1} cm^{-1})): 877 (1,390), 499 (9,990); IR, *v*(C≡C) (cm^{-1}): 2078(s); Electrochemistry, $E_{1/2}$ (V), ΔE_p (V), $i_{backward}/i_{forward}$: **A**, 0.503, 0.063, 0.915; **B**, −1.106, 0.059, 0.742; **C**, −2.143, N/A, N/A; **D**, −1.501, N/A, N/A.

Preparation of Ru_2(DiMeODMBA)$_4$(C_2TMS)$_2$ (**3b**) was undertaken using the same procedure as that for **2b** and replacing LiC_2Ph with LiC_2TMS in 93% yield. Data for **3b**: ^{1}H-NMR: 6.48–6.44 (*m*, 4H, aromatic), 6.16–5.92 (*m*, 8H, aromatic), 3.76 (*s*, 24H, CH_3O–), 3.25 (*s*, 24H, CH_3N–), 0.10 (s, 18H, (CH_3)$_3$Si–); ^{13}C-NMR (C≡C): 125.9, 99.7; FABMS (*m*/*e*, based on ^{101}Ru): 1226 [M^+H]; Vis–NIR, λ_{max} (nm, ε (M^{-1} cm^{-1})): 855 (840), 490 (5,330); IR, *v*(C≡C) (cm^{-1}): 2006(s); Electrochemistry, $E_{1/2}$ (V), ΔE_p (V), $i_{backward}/i_{forward}$: **A**, 0.559, 0.082, 0.964; **B**, −1.150, 0.055, 0.468; **C**, −2.283, N/A, N/A; **D**, −1.491, N/A, N/A.

Preparation of Ru_2(DiMeODMBA)$_4$(C_2Tips)$_2$ (**4b**) was undertaken using the same procedure as that for **2b** and replacing LiC_2Ph with LiC_2Tips in 95% yield. Data for **4b**: ^{1}H-NMR: 6.44 (*t*, 4H, aromatic), 6.07 (*d*, 8H, aromatic), 3.75 (*s*, 24H, CH_3O–), 3.27 (*s*, 24H, CH_3N–), 0.96, 0.89 (m, 42H, (C_3H_7)$_3$Si–); ^{13}C-NMR (C≡C): 130.8, 60.8; FABMS (*m*/*e*, based on ^{101}Ru): 1394 [M^+H]; Vis–NIR, λ_{max} (nm, ε (M^{-1} cm^{-1})): 858 (1,290); IR, *v*(C≡C) (cm^{-1}): 2002(s); Electrochemistry,

$E_{1/2}$ (V), ΔE_p (V), $i_{backward}/i_{forward}$: **A**, 0.586, 0.066, 0.953; **B**, −1.151, 0.054, 0.685; **C**, −2.356, N/A, N/A; **D**, −1.510, N/A, N/A.

Preparation of $Ru_2(DiMeODMBA)_4(C_4TMS)_2$ (**5b**) was undertaken using the same procedure as that for **2b** and replacing LiC_2Ph with LiC_4TMS. Silica column chromatography was used to separate **5b** (70%) from trace amounts of *trans*-$(TMSC_4)Ru_2(DiMeODMBA)_4(C_4H)$ and $Ru_2(DiMeODMBA)_4(C_4H)_2$. Data for **5b**: Anal. for $C_{58}H_{78}N_8O_8Ru_2Si_2\cdot 2H_2O$ Found (Calc.): C, 52.66 (52.89); H, 6.04 (6.23); N, 8.41 (8.51)%. ^{1}H-NMR: 6.45 (*t*, 4H, aromatic), 6.03 (*d*, 8H, aromatic), 3.75 (*s*, 24H, CH_3O–), 3.20 (*s*, 24H, CH_3N–); ^{13}C-NMR (C≡C): 108.8, 90.1, 76.0, 70.6; FABMS (*m*/*e*, based on ^{101}Ru): 1274 [M$^+$H]; Vis–NIR, λ_{max} (nm, ε (M^{-1} cm^{-1})): 878 (1,590), 512 (8,930); IR, ν(C≡C) (cm^{-1}): 2117(*s*), 2020(*w*); Electrochemistry, $E_{1/2}$ (V), ΔE_p (V), $i_{backward}/i_{forward}$: **A**, 0.725, 0.060, 0.887; **B**, −0.900, 0.058, 0.703; **C**, −1.921, N/A, N/A; **D**, −1.308, N/A, N/A.

Preparation of $Ru_2(DEBA)_4(C_2Ph)_2$ (**2c**). To a 40 ml THF solution of $Ru_2(DEBA)_4Cl_2$ (0.360 g, 0.37 mmol) was added 5 equiv. of LiC_2Ph at r.t. The reaction mixture was stirred under argon for 2 h, followed by filtration through a silica pad to yield a dark red solution. After solvent removal, the residue was washed with copious amount of methanol and hexanes and dried under vacuum overnight to yield **2c** as red crystalline solid (0.327 g, 80%). Data for **2c**: ^{1}H-NMR: 7.46–7.43 (*m*, 10H, aromatic), 7.27–7.22 (*d*, 8H, aromatic), 7.17–7.14 (*t*, 6H, aromatic), 7.06 (*d*, 4H, aromatic), 6.90 (*t*, 2H, aromatic), 4.05 (*s*, 16H, CH_3CH_2N–), 0.99 (*t*, 24H, CH_3CH_2N–); ^{13}C-NMR (C≡C): 105.2, 63.4; FABMS (*m*/*e*, based on ^{101}Ru): 1106 [M$^+$H]; Vis–NIR, λ_{max} (nm, ε (M^{-1} cm^{-1})): 846 (1,060), 507 (7,970); IR, ν(C≡C) (cm^{-1}): 2081(*s*); Electrochemistry, $E_{1/2}$ (V), ΔE_p (V), $i_{backward}/i_{forward}$: **A**, 0.575, 0.070, 0.954; **B**, −1.036, 0.051, 0.230; **C**, −2.211, N/A, N/A; **D**, −1.468, 0.063, 0.634.

Preparation of $Ru_2(DEBA)_4(C_2TMS)_2$ (**3c**) was undertaken using the same procedure as that for **2c** and replacing LiC_2Ph with LiC_2TMS in 79% yield. Data for **3c**: ^{1}H-NMR: 7.42–7.36 (*m*, 12H, aromatic), 7.17–7.11 (*m*, 8H, aromatic), 3.9 (*s*, 16H, CH_3CH_2N–), 0.88 (*t*, 24H, CH_3CH_2N–); ^{13}C-NMR (C≡C): 94.8, 68.4; FABMS (*m*/*e*, based on ^{101}Ru): 1097 [M$^+$H]; Vis–NIR, λ_{max} (nm, ε (M^{-1} cm^{-1})): 829 (1,880), 504 (12,920); IR, ν(C≡C) (cm^{-1}): 2006; Electrochemistry, $E_{1/2}$ (V), ΔE_p (V), $i_{backward}/i_{forward}$: **A**, 0.625, 0.061, 0.985; **B**, −1.085, 0.049, 0.270; **C**, N/A, N/A, N/A; **D**, −1.487, 0.079, 0.468.

Preparation of $Ru_2(DEBA)_4(C_2Tips)_2$ (**4c**) was undertaken using the same procedure as that for **2c** and replacing LiC_2Ph with LiC_2Tips in 73% yield. Data for **4c**: Anal. for $C_{66}H_{102}N_8Ru_2Si_2\cdot 2H_2O$ Found (Calc.): C, 60.52 (60.92); H, 8.30 (8.15); N, 8.53 (8.62)%. ^{1}H-NMR: 7.54–7.02 (*m*, 20H, aromatic), 4.51 (*s*, 16H, CH_3CH_2N–), 1.50–0.85 (*m*, 66H, CH_3CH_2N– and $Si(C_3H_7)_3$); ^{13}C-NMR (C≡C): 92.2, 55.5; FABMS (*m*/*e*, based on ^{101}Ru): 1268 [M$^+$H]; Vis–NIR, λ_{max} (nm, ε (M^{-1} cm^{-1})): 801 (910), 502 (5,710); IR, ν(C≡C) (cm^{-1}): 1996(*s*); Electrochemistry, $E_{1/2}$ (V), ΔE_p (V), $i_{backward}/i_{forward}$: **A**, 0.680, 0.059, 0.907; **B**, −1.075, 0.069, 0.845; **C**, N/A, N/A, N/A; **D**, −1.481, 0.077, 0.711.

Preparation of $Ru_2(DEBA)_4(C_4TMS)_2$ (**5c**) was carried out using the same procedure as that for **2c** and replacing LiC_2Ph with LiC_4TMS. Silica column chromatography was used to separate **5c** (72%) from trace amounts of *trans*-$(TMSC_4)Ru_2(DEBA)_4(C_4H)$ and $Ru_2(DEBA)_4(C_4H)_2$. Data for **5c**: Anal. for $C_{58}H_{78}N_8Ru_2Si_2\cdot CH_2Cl_2\cdot H_2O$ Found (Calc.): C, 56.43 (56.78); H, 6.78 (6.58); N, 8.53 (8.98)%. ^{1}H-NMR: 7.44–7.32 (*m*, 12H, aromatic), 7.22–7.16 (*m*, 8H, aromatic), 3.93 (*s*, 16H, CH_3CH_2N–), 0.96 (*t*, 24H, CH_3CH_2N–), 0.08 (s, 18H, $Si(CH_3)_3$); ^{13}C-NMR (C≡C): 136.3, 110.7, 94.7, 65.3; FABMS (*m*/*e*, based on ^{101}Ru): 1146 [M$^+$H]; Vis–NIR, λ_{max} (nm, ε (M^{-1} cm^{-1})): 849 (1,980), 520 (12,970); IR, ν(C≡C) (cm^{-1}): 2162(*m*), 2107(*s*); Electrochemistry, $E_{1/2}$ (V), ΔE_p (V), $i_{backward}/i_{forward}$: **A**, 0.777, 0.065, 0.791; **B**, −0.860, 0.040, 0.798; **C**, −1.903, N/A, N/A; **D**, −1.337, 0.046, 0.321.

X-ray data collection, processing, and structure analysis and refinement. Single crystals of **1b**, **1c**, **2c**, **3c** and **4b** were grown via either slow evaporation (THF–hexanes solution for **2c**, **3c**, **4b**, and CH_2Cl_2–hexanes solution for **1b**) or slow cooling of a THF–hexanes solution (**1c**). X-ray intensity data were measured at 300 K on a Bruker SMART1000 CCD-based X-ray diffractometer system using Mo–K_α ($\lambda = 0.71073$ Å). Crystals used for X-ray crystallographic analysis were cemented onto a quartz fiber with epoxy glue. Data were measured using omega scans of 0.3° per frame such that a hemisphere (1271 frames) was collected. No decay was indicated for either data set by the recollection of the first 50 frames at the end of each data collection. The frames were integrated with the Bruker SAINT© software package [29] using a narrow-frame integration algorithm, which also corrects for the Lorentz and polarization effects. Absorption corrections were applied using SADABS supplied by George Sheldrick.

Structures were solved and refined using the Bruker SHELXTL© (Version 5.1) software package [30–32] in the space groups $P2_1/n$ (**1b**), $I422$ (**1c**), $P2_1/n$ (**2c**), $Aba2$ (**3c**) and $P\bar{1}$ (**4b**). Positions of all non-hydrogen atoms of diruthenium moieties were revealed by direct method. With all non-hydrogen atoms being anisotropic and all hydrogen atoms in calculated position and riding mode the structure was refined to convergence by least squares method on F^2 (SHELXL-93, incorporated in SHELXTL.PC v 5.03). Relevant information on the data collection and

Table 5
Crystal data for compounds **1b**, **1c**, **2c**, **3c** and **4b**

	1b·$2CH_2Cl_2$	**1c**	**2c**	**3c**	**4b**
Formula	$C_{46}H_{64}Cl_6N_8O_8Ru_2$	$C_{44}H_{60}Cl_2N_8Ru_2$	$C_{60}H_{70}N_8Ru_2$	$C_{54}H_{78}N_8Ru_2Si_2$	$C_{66}H_{102}N_8O_8Ru_2Si_2$
Formula weight	1271.9	974.0	1105.38	1097.6	1393.9
T (K)	300	300	300	300	300
Crystal system	Monoclinic	Tetragonal	Monoclinic	Orthorhombic	Triclinic
Space group	$P2_1/n$	$I\bar{4}22$	$P2_1/n$	$Aba2$	$P\bar{1}$
a (Å)	14.394(2)	14.163(2)	12.432(1)	17.460(2)	11.9822(8)
b (Å)	27.729(4)		17.394(2)	21.944(3)	12.6886(8)
c (Å)	14.561(2)	11.921(2)	13.667(1)	14.803(1)	13.6137(9)
α (°)					65.449(1)
β (°)	91.968(3)		113.105(1)		78.140(1)
γ (°)					67.024(1)
V (Å^3)	5808(2)	2391.1(6)	2718.2(5)	5672(1)	1731.0(2)
Z	4	2	2	4	1
ρ_{calc} (g cm^{-3})	1.455	1.353	1.351	1.285	1.337
μ (mm^{-1})	0.849	0.781	0.601	0.615	0.528
Crystal size (mm)	0.26 × 0.13 × 0.02	0.27 × 0.26 × 0.21	0.18 × 0.12 × 0.02	0.13 × 0.11 × 0.05	0.17 × 0.12 × 0.02
Reflections measured	30 019	6118	14 228	14 606	9048
Unique reflections (R_{int})	10 197 (0.156)	1068 (0.061)	4787 (0.043)	4952 (0.029)	6020 (0.025)
Parameters refined	644	67	374	305	402
R, wR_2 ($I > 2\sigma(I)$)	0.083, 0.164	0.038, 0.122	0.054, 0.148	0.032, 0.071	0.046, 0.100
Goodness-of-fit on F^2	1.01	0.99	1.00	1.00	1.01

the figures of merit of final refinement are listed in Table 5.

5. Supplementary material

Crystallographic data for the structural analysis have been deposited with the Cambridge Crystallographic Data Center, CCDC Nos. 209248–209252 for compounds **1b**, **1c**, **2c**, **3c** and **4b**, respectively. Copies of this information may be obtained free of charge from The Director, CCDC, 12 Union Road, Cambridge CB2 1EZ, UK (Fax: +44-1223-336033; e-mail: deposit@ccdc.cam.ac.uk or www: http://www.ccdc.cam.ac.uk). Vis–NIR spectra (compounds **1**–**5**, Figures S1–S3) and CV plots (**1b**–**5b** and **1c**–**5c**, Figures S4 and S5) are also available in the supporting information.

Acknowledgements

We thank both the National Science Foundation (CHE 0242623) and the University of Miami (CCD-diffractometer fund) for financial support. G.-L. Xu is a Maytag Graduate Fellow at the University of Miami.

References

[1] T. Ren, G.-L. Xu, Comments Inorg. Chem. 23 (2002) 355.
[2] T. Ren, G. Zou, J.C. Alvarez, Chem. Comm. (2000) 1197.
[3] G.-L. Xu, G. Zou, Y.-H. Ni, M.C. DeRosa, R.J. Crutchley, T. Ren, J. Am. Chem. Soc. 125 (2003) 10057.
[4] T. Ren, Organometallics 21 (2002) 732.
[5] G.-L. Xu, T. Ren, J. Organomet. Chem. 655 (2002) 239.
[6] G.-L. Xu, T. Ren, Organometallics 20 (2001) 2400.
[7] S.K. Hurst, T. Ren, J. Organomet. Chem. 660 (2002) 1.
[8] G. Zou, J.C. Alvarez, T. Ren, J. Organomet. Chem. 596 (2000) 152.
[9] G.-L. Xu, T. Ren, Inorg. Chem. 40 (2001) 2925.
[10] C. Lin, T. Ren, E.J. Valente, J.D. Zubkowski, J. Chem. Soc. Dalton Trans. (1998) 571.
[11] C. Lin, T. Ren, E.J. Valente, J.D. Zubkowski, J. Organomet. Chem. 579 (1999) 114.
[12] G.-L. Xu, C. Campana, T. Ren, Inorg. Chem. 41 (2002) 3521.
[13] V.W.-W. Yam, Acc. Chem. Res. 35 (2002) 555.
[14] N.J. Long, in: D.M. Roundhill, J.P. Fackler (Eds.), Optoelectronic Properties of Inorganic Compounds, Plenum Press, New York, 1999.
[15] F.A. Cotton, C. Lin, C.A. Murillo, Acc. Chem. Res. 34 (2001) 759.
[16] J.-L. Zuo, F.F.d. Biani, A.M. Santos, K. Köhler, F.E. Kühn, Eur. J. Inorg. Chem. (2003) 449.
[17] J.-L. Zuo, E. Herdtweck, F.F.d. Biani, A.M. Santos, F.E. Kühn, New J. Chem. 26 (2002) 889.
[18] J.-L. Zuo, E. Herdtweck, F.E. Kühn, J. Chem. Soc. Dalton Trans. (2002) 1244.
[19] G.-L. Xu, T. Ren, unpublished results.
[20] J.L. Bear, B. Han, S. Huang, K.M. Kadish, Inorg. Chem. 35 (1996) 3012.
[21] J. Emsley, The Elements, Oxford University Press, Oxford, 1991.
[22] F.A. Cotton, A. Yokochi, Inorg. Chem. 36 (1997) 567.
[23] F.A. Cotton, R. A. Walton, Multiple Bonds between Metal Atoms, Oxford University Press, Oxford, 1993.
[24] T. Ren, Coord. Chem. Rev. 175 (1998) 43.
[25] U.H.F. Bunz, Chem. Rev. 100 (2000) 1605.
[26] K. Mullen, G. Wegner, Electronic Materials: The Oligomer Approach, Wiley-VCH, Weinheim, New York, 1998.
[27] A. Bino, F.A. Cotton, W. Kaim, Inorg. Chem. 18 (1979) 3566.
[28] W.-Z. Chen, G.-L. Xu, C.G. Jablonski, T. Ren, Tetrahedron, manuscript in preparation.

[29] SAINT V 6.035 Software for the CCD Detector System, Bruker-AXS Inc., 1999.
[30] SHELXTL 5.03 (WINDOW-NT Version), Program library for Structure Solution and Molecular Graphics, Bruker-AXS Inc., 1998.
[31] G.M. Sheldrick, SHELXS-90, Program for the Solution of Crystal Structures, University of Göttigen, Germany, 1990.
[32] G.M. Sheldrick, SHELXL-93, Program for the Refinement of Crystal Structures (1993) University of Göttigen, Germany.